THE JOURNAL OF PHYSICAL CHEMISTRY B

Article

pubs.acs.org/JPCB

Improved Self-Healing of Polyethylene/Carbon Black Nanocomposites by Their Shape Memory Effect

Xiaoyan Wang,[†] Jun Zhao,*[,†] Min Chen,[†] Lan Ma,[‡] Xiaodong Zhao,[†] Zhi-Min Dang,[†] and Zhenwen Wang[†]

[†]Department of Polymer Science and Engineering, School of Chemistry and Biological Engineering, University of Science and Technology Beijing, Beijing 100083, P. R. China

[‡]Department of Chemical Engineering, Texas Tech University, Lubbock, Texas 79409, United States

ABSTRACT: In this work, the improved self-healing of cross-linked polyethylene (PE) (*c*PE)/carbon black (CB) nanocomposites by their shape memory effect (SME) is investigated. CB nanoparticles are found to be homogeneously dispersed in the PE matrix and significantly increase the strength of the materials. Compared with the breaking of linear PE (*l*PE) at the melting temperature (T_m), the *c*PE and *c*PE/CB nanocomposites still have high strength above T_m due to the formation of networks. The *c*PE and *c*PE/CB nanocomposites show both high strain fixity ratio (R_f) and high strain recovery ratio (R_r). Crystallization-induced elongation is observed for all the prepared shape memory polymer (SMP) materials and the effect becomes less remarkable with increasing volume fraction of CB nanoparticles (v^{CB}). The scratch self-healing tests show that the cross-linking of PE matrix, the addition of CB nanoparticles, and the previous stretching in the direction perpendicular to the scratch favor the closure of the scratch and its complete healing. This SME-aided self-healing could have potential applications in diverse fields such as coating and structure materials.

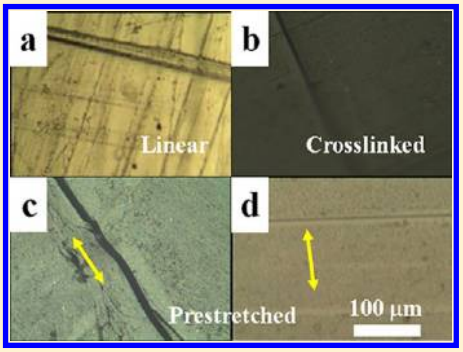

INTRODUCTION

Smart polymer materials such as shape memory polymers (SMPs) and self-healing polymers (SHPs) can sense and respond to the external stimuli such as temperature, force, light, sound, electricity, pH change, and humidity change.[1,2] Besides, most of the smart polymer materials have excellent mechanical, thermal, and corrosion-resistant properties, good processability, and low cost. Therefore, such materials have good potential to be used in spacecrafts, biology, medicine, industry, and daily lives.

SMPs are the polymer materials that can memorize the permanent shape by holding the temporary shape after deformation, and then recovering to its permanent shape under external stimulus.[2] Compared with shape memory alloys (SMAs) and shape memory ceramics (SMCs), SMPs have many advantages such as the ability to sustain high strain (up to 500−800%), low response temperature, tunable elastic modulus, and low density.[2−7] SMPs are generally composed of two phases: one is the fixed phase that can be chemical or physical cross-linking points and is used to hold the permanent shape, and the other is the reversible phase that can be amorphous or crystalline phase and is used to change and recover the shape. When the temperature is above the switch temperature (T_{sw}) such as glass transition temperature (T_g) and melting temperature (T_m), the molecular chains in the reversible phase can move under the external force such as tension and change the shape from curled to stretched. Then the strain can be frozen by cooling to temperatures below T_{sw} under the external force. When the force is unloaded, usually the strain has a slight decrease. Finally, the molecular chains can release the strain and recover to the permanent shape when the temperature is increased above T_{sw} without external force.

The current hot topics in the field of SMP are as follows: SMP composites to increase the mechanical and thermal properties and biocompatibility and remote triggering,[8−16] SMP with biocompatibility to be used in medical field,[7,17−19] SMP with reversible shape memory effect (SME) to be used as artificial muscles,[20] and SMP with triple and multiple SMEs to provide complex actuation.[15,21−25]

SHPs are the materials that can heal the microcracks produced during the use in a way like the biological system that can heal the wound.[1] The microcracks produced in different materials will deteriorate the mechanical, thermal, and electrical properties, and accelerate the damage process. But it cannot be easily detected or repaired. Therefore, the lifetime of ceramics, metal, and polymer materials can be prolonged if the self-healing is achieved, which will reduce the economic loss caused by renewing the materials. Self-healing ability is even more important and crucial for the polymers and their composites because of their rapidly increasing use in both industry and daily lives nowadays.[1]

So far, there have been four main methods for the self-healing of polymer materials: microcapsules, microvascular networks (or hollow fibers), thermoplastic additives, and reversible

Received: October 6, 2012
Revised: December 2, 2012
Published: January 9, 2013

 © 2013 American Chemical Society dx.doi.org/10.1021/jp3098796 | *J. Phys. Chem. B* 2013, 117, 1467−1474

reactions.[1] Among these methods, only the last one does not need the addition of healing agent to the polymer matrix. For the microcapsule method, the liquid healing agent is sealed in the microcapsules which are dispersed in the matrix. When the microcrack penetrates the microcapsules, the liquid healing agent will be released.[26,27] For the microvascular network method which is similar to the microcapsule method, the liquid healing agent is sealed in the hollow fibers.[28] The thermoplastic additive method is by the physical adhesion between the molten thermoplastic additives and the polymer matrix.[29] As for the reversible reaction method, the reaction can be thermally reversible reaction, ionic coupling, molecular dispersing, and the formation of hydrogen bonds.[30−35] Although these methods are successful in some specific applications, each of them has some limitations. For example, the microcapsule and microvascular network methods can be used only once rather than repeatedly. The reversible reaction method has special requirement on the chemical structures of polymer matrix and thus it is not a universal method. As for the thermoplastic additive method, usually a large amount of additives up to 40 vol % is needed to fill in the macroscopic cracks produced simultaneously with the occurrence of microcraks. Clearly, such a great amount of thermoplastic additives will inevitably damage the properties of the polymer matrix. Recently, a new strategy of self-healing based on the SME has been proposed to first close the macroscopic cracks before the thermoplastic additives are used to fill in the microcracks.[36−38] In this way, the amount of healing agent can be reduced significantly and the properties of the matrix can be preserved to a high extent. Actually, there is also a limitation that the whole polymer matrix needs to be cross-linked.

The main purpose of this work is to improve the self-healing effect by using SME in a different way from what has been reported in the literature. Polyethylene (PE) is chosen as the polymer matrix because it is one of the most important polyolefins and a general plastic with a giant cost advantage. The recent improvements in the synthesis and processing have given the polyolefins better chemical and microscopic structures, which makes them excellent candidate to replace the traditional steel and iron materials in the pipeline and automobile industry. Carbon black (CB) nanoparticles are chosen as the reinforcing and conductive nanofillers because of their common use, low cost, and high chemical stability.

EXPERIMENTAL METHODS

Materials. PE (type LD100BW) pellets with density of 0.923 g cm^{-3} and melt flow index of 2.0 g $(10\ min)^{-1}$ were supplied by Sinopec Beijing Yanshan Co. (China). CB nanoparticles (Vulcan XC68) with diameter of 30−50 nm, iodine number of 68 mg g^{-1}, and dibutyl phthalate number (DBP) of 123 mL (100 g^{-1}) were purchased from Cabot Corp. (USA). 2,5-Dimethyl-2,5-di(*tert*-butylperoxy)hexane (DHBP, 92%) was supplied by Acros Organics (Belgium). Xylene (AR) was purchased from Beijing Chemical Plant (China).

Sample Preparation. PE pellets and CB nanoparticles were dried completely in a vacuum oven at 80 °C overnight before use. PE and CB nanoparticles with various volume ratios were added to and mixed in a Thermal Scientific Haake MiniLab II mixer (Germany) at 140 °C and 60 rpm for 10 min. Then, the mixtures were extruded and cut into pieces before they were soaked by DHBP in a hermetic glass flask at room temperature for 72 h. Subsequently, the soaked mixtures were molded by hot pressing at 200 °C and 20 MPa for 30 min to get the cross-linking of PE. Finally, thin films with thickness of 0.5−1.0 mm were obtained by slow cooling in air.

Gel Fraction (f_g) Measurements. Samples of 0.05−0.1 g were immersed in large volume of xylene and stirred gently at 95 °C to selectively extract the un-cross-linked linear PE (*l*PE) component until the samples reached a constant weight. Then the extracted samples were dried completely in a vacuum oven at 80 °C and the weight was checked. The equation of the quantitative data on the f_g is as follows

$$f_g = \frac{w_f}{w_i} \times 100\% \quad (1)$$

where w_i and w_f are the weights of the sample before and after the extraction. The f_g represents the fraction of cross-linked PE (*c*PE) component in the sample. The reported value was the average of at least three samples with the same composition and the same processing conditions.

Scanning Electron Microscopy (SEM) Observation. The samples were fractured in liquid nitrogen and then the fractured surface was sputtered with carbon. Morphology observation was performed on a Zeiss Evo 18 Special Edition SEM (Germany) with accelerating voltage of 20 kV.

Differential Scanning Calorimetry (DSC) Measurements. DSC measurements were carried out using a DSC-60 (Shimadzu, Japan) in nitrogen atmosphere. Temperature and enthalpy were calibrated with indium. The samples of 5−10 mg were dried in a vacuum oven at 80 °C before they were sealed in aluminum crucibles. The samples were heated from room temperature to 200 °C at 10.0 K min^{-1}.

Dielectric Measurements. Samples of cylindrical shape with circle area of ca. 1.0 cm^2 and thickness of 0.5−1.0 mm were prepared by hot pressing as mentioned above for the dielectric measurements. Both sides of the samples were coated with silver as electrodes. The dielectric measurements were performed on an Agilent 4294A impedance analyzer (USA) over the frequency range of 10^2−10^7 Hz and the temperatures range of −50 to 150 °C with heating rate of ca. 1.0 K min^{-1}.

Dynamic Mechanical Thermal Analysis (DMTA) Measurements and Shape Memory Analysis. The traditional DMTA measurements were performed on a dynamic mechanical thermal analyzer (TA Instruments Q800, USA) in the tension mode with the temperature range from room temperature to 200 °C, heating rate of 3.0 K min^{-1}, and frequency of 1 Hz. The samples had a width of ca. 3.0 mm and a thickness of 0.5−1.0 mm. The initial clamp gap was ca. 5.0 mm and the strain was 0.05%. It should be mentioned that the low heating/cooling rate of 3.0 K min^{-1} is employed in DMTA measurements to avoid serious temperature gradient.

For the shape memory analysis of the prepared SMP samples, a four-step program on the dynamic mechanical thermal analyzer was employed. In the first step, the samples were heated rapidly to 130.0 °C and kept isothermal at the temperature for 3 min, and then the samples were stretched from 0 to 1 at 0.1 N min^{-1}. In the second step, the samples were cooled at 3.0 K min^{-1} under the force of 1 N. In the third step, the force was removed at 0.05 N min^{-1}. In the last step, the samples were heated to 130.0 °C at 3.0 K min^{-1}. This cycle was repeated several times to check the reproducibility of SME.

Two important quantities to describe the SME of the samples are the strain fixity ratio (R_f) and strain recovery ratio (R_r) as follows[39]

$$R_f = \frac{\varepsilon_{rem}}{\varepsilon_{pr}} \times 100\% \quad (2)$$

dx.doi.org/10.1021/jp3098796 | J. Phys. Chem. B 2013, 117, 1467−1474

$$R_r = \frac{\varepsilon_{pr} - \varepsilon_{rec,m}}{\varepsilon_{pr}} \times 100\% \quad (3)$$

where ε_{pr} (programming strain) is the strain (ε) after the second step, ε_{rem} (remaining strain) is that after the third step, and $\varepsilon_{rec,m}$ (residual strain) is that after the fourth step.

Self-Healing Tests. The prepared SMP films with width of ca. 0.5−1.0 mm were stretched by an ε of ca. 50% on a hot stage at ca. 140 °C and then slowly cooled to room temperature under the force. Then the force was removed and a sharp blade was used for the films' single surface to make a straight scratch with width of ca. 20−40 μm, depth of 5−10 μm, and length of ca. 5 mm in the direction parallel or perpendicular to the previous stretching direction. For comparison, such a scratch was also made on the surface of unstretched *l*PE, *c*PE, and *c*PE/CB nanocomposites with various volume fraction of CB nanoparticles (v^{CB}). Subsequently, the samples were heated from room temperature to 150.0 °C at 10.0 K min^{-1} on a hot stage (Yudian Al-708, China) and the evolution of the scratch was recorded by an optical microscope (OM) (Leitz Ortholux 2 Pol, Germany) equipped with CCD.

Table 1. Properties of *c*PE and *c*PE/CB Nanocomposites with Various v^{CB}[a]

	v^{CB} (vol %)				
	0	1.0	5.0	10.0	20.0
f_g (%)	98.6	99.2	99.3	98.7	98.2
ε_b (%)	107.0	120.7	136.5	82.3	79.1
R_f (%)	93.6	93.2	91.9	89.2	85.1
R_r (%)	99.7	99.6	99.7	99.4	99.0

[a] v^{CB}, f_g, ε_b, R_f, and R_r are volume fraction of CB nanoparticles, gel fraction, strain at break, strain fixity ratio, and strain recovery ratio, respectively.

RESULTS AND DISCUSSION

DHBP with two peroxy groups is employed as a cross-linking agent for PE samples because of its fluidity at room temperature, high thermal stability at temperature up to 145 °C, and high reaction efficiency at higher temperature of 200 °C.[14,22,39] The cross-linking reaction occurs by the decomposition of DHBP to produce two reactive oxygen radicals, which can react

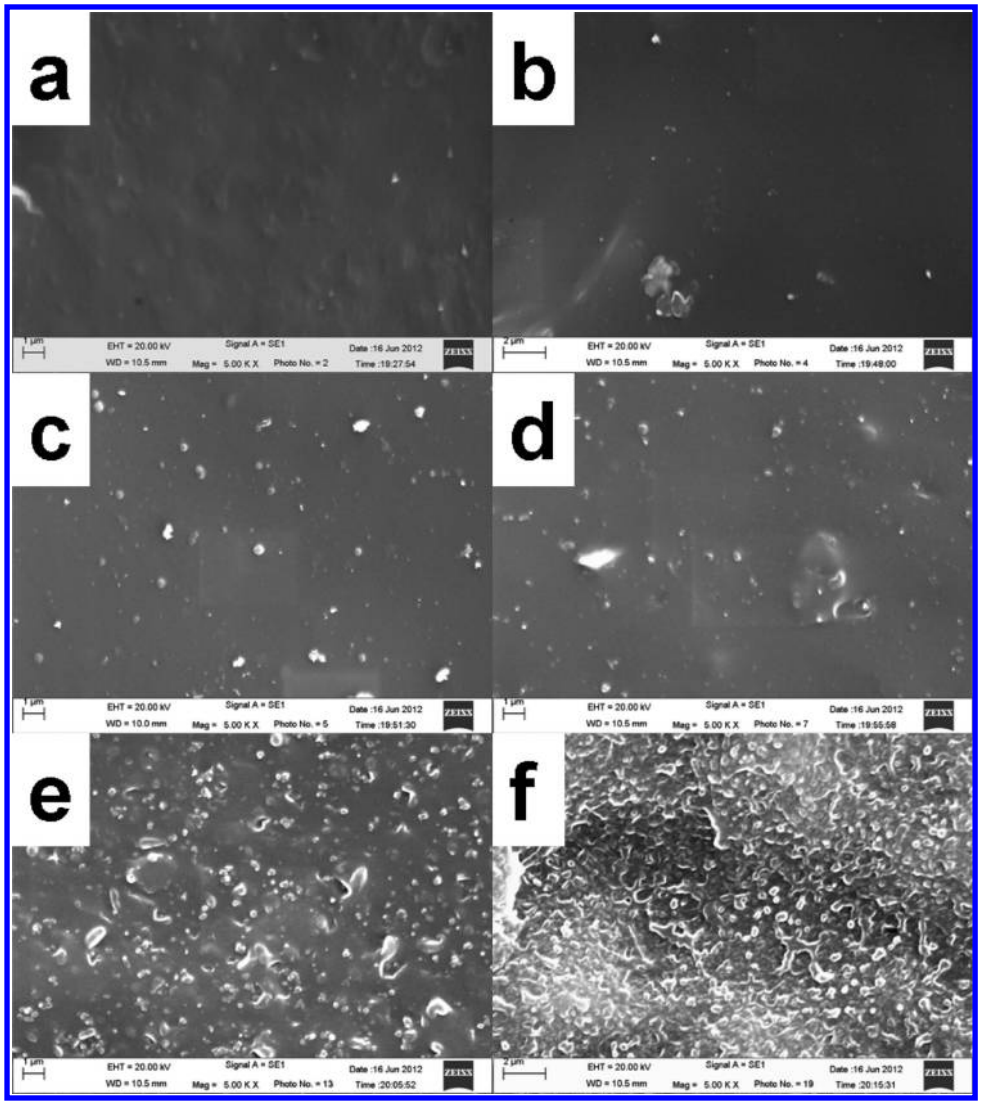

Figure 1. SEM micrographs of the cryo-fractured surface of *l*PE (a), *c*PE (b), and *c*PE/CB nanocomposites with various v^{CB}: 0.5 (c), 1.0 (d), 5.0 (e), and 20.0 vol % (f).

dx.doi.org/10.1021/jp3098796 | J. Phys. Chem. B 2013, 117, 1467−1474

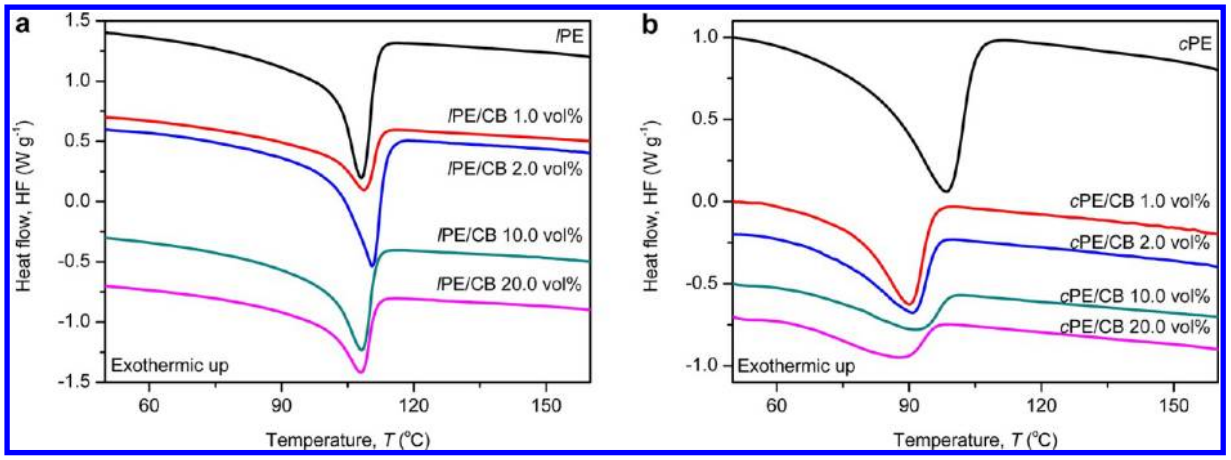

Figure 2. DSC thermographs showing HF of *l*PE/CB (a) and *c*PE/CB (b) nanocomposites with various ν^{CB} as indicated beside each curve.

with and connect different PE chains. As given in Table 1, the f_g of all the prepared *c*PE and *c*PE/CB nanocomposites with various ν^{CB} is high (above 98%), which means that the cross-linking reaction of PE matrix happens and almost complete PE networks are formed in the system. Therefore, SMP materals based on *c*PE/CB nanocomposites are successfully prepared.

Figure 1 presents the SEM micrographs of the cryo-fractured surface of *l*PE, *c*PE, and *c*PE/CB nanocomposites. It can be seen that the surface of *c*PE is smoother than that of the *l*PE due to the polymer networks formed in the former. For the *c*PE/CB nanocomposites, homogeneous dispersion of CB nanoparticles in the system can be seen for the ν^{CB} up to 20.0 vol %. Actually, for the *c*PE/CB nanocomposites with ν^{CB} of 20.0 vol %, the CB nanoparticles already form percolation networks in the system as will be proved by the dielectric measurements below. The rough surface of this sample might be due to not only the high ν^{CB} but also the increased ductility caused by the fillers.[40]

Figure 2 presents the DSC heat flow (HF) traces of *l*PE/CB and *c*PE/CB nanocomposites. It can be seen that, for all the samples, there is only a single melting peak appearing at ca. 90−110 °C. For the *l*PE/CB nanocomposites, the T_m increases slightly with increasing ν^{CB} up to 2.0 vol % and then decreases with further increasing ν^{CB}. This can be explained by the nucleation effect of CB nanoparticles on the crystallization of PE for the low ν^{CB} and the disturbance effect of the fillers to the crystallization for the high ν^{CB}. For the *c*PE/CB nanocomposites, the T_m decreases monotonically and the melting peak becomes broader with increasing ν^{CB}. This should be due to the combination of the different cross-linking degrees and the fillers' nucleation and disturbance effect.

Figure 3 presents the temperature dependence of storage dielectric constant (ε') in *l*PE, *c*PE, and *c*PE/CB nanocomposites at 10^4 Hz. It can be seen that for the *l*PE, *c*PE, and *c*PE/CB nanocomposites with ν^{CB} up to 5.0 vol %, there is a step at ca. 95 °C, which corresponds to the melting of PE matrix. But for the *c*PE/CB nanocomposites with ν^{CB} of 10.0 vol %, this step shifts down to ca. 70 °C. Compared with *l*PE, *c*PE has a little bit higher ε'. The ε' of cPE/CB nanocomposites further increases with increasing ν^{CB}. There is a sharp jump in ε' when the ν^{CB} is increased from 5.0 to 10.0 vol %. In our experiments, the sample with ν^{CB} of 20.0 vol % is actually conducting. Therefore, the percolation threshold for this system is between 10.0 and 20.0 vol %.

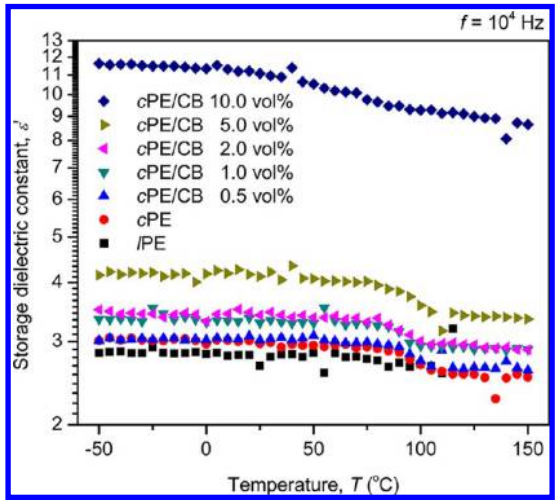

Figure 3. Temperature dependence of ε' in *l*PE, *c*PE, and *c*PE/CB nanocomposites with various ν^{CB} at 10^4 Hz.

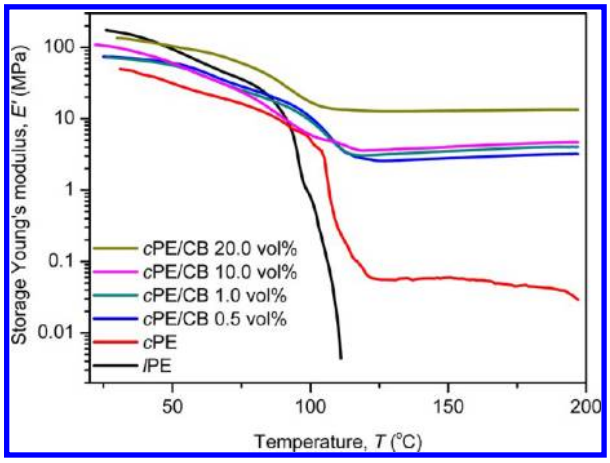

Figure 4. Temperature dependence of E' in *l*PE, *c*PE, and *c*PE/CB nanocomposites with various ν^{CB}.

Figure 4 presents the temperature dependence of storage Young's modulus (E') in *l*PE, *c*PE, and *c*PE/CB nanocomposites. A pronounced difference between *l*PE and *c*PE and *c*PE/CB nanocomposites can be seen: the E' falls down to 0 at ca. 110 °C for the *l*PE, while it just decreases to a lower value above 0 for both *c*PE and *c*PE/CB nanocomposites.

dx.doi.org/10.1021/jp3098796 | J. Phys. Chem. B 2013, 117, 1467−1474

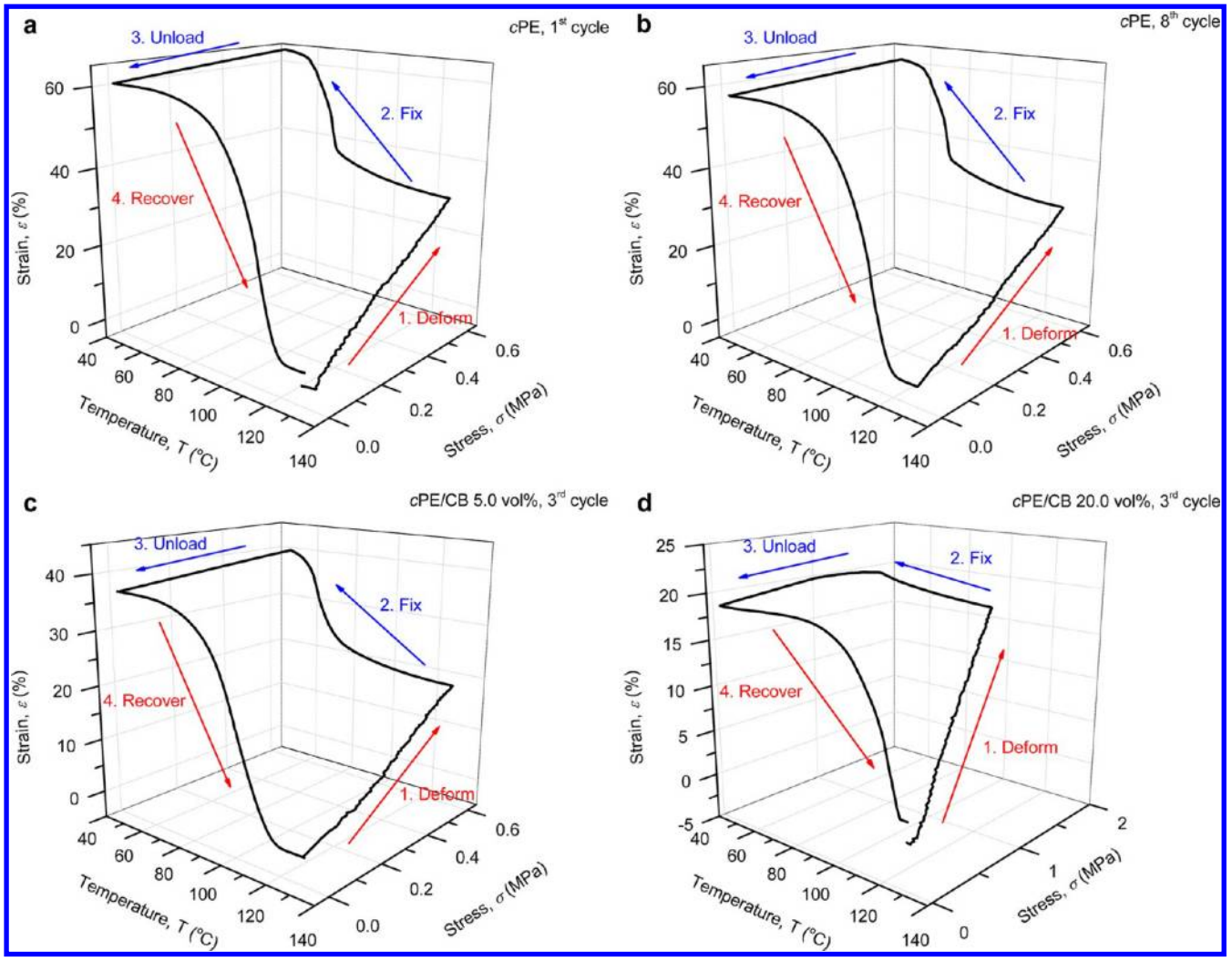

Figure 5. 3D diagram of shape memory cycle of *c*PE for the first (a) and eighth (b) cycle and *c*PE/CB nanocomposites with v^{CB} of 5.0 (c) and 20.0 vol % (d) for the third cycle.

The reason for the E' decrease in all the samples can be attributed to the melting of PE matrix. For the *c*PE and *c*PE/CB nanocomposites, the E' step is due to the formation of cross-linked networks in the system. For the temperature below the T_m, there is no clear trend of E' due to the combined effects of cross-linking degree and crystallinity. However, for the temperature above the T_m, the E' increases continuously with increasing v^{CB} due to the combined effects of matrix's cross-linking and fillers' reinforcing effect. Table 1 also shows that the ε at break (ε_b) for all the *c*PE and *c*PE/CB nanocomposites is around 100%, which is in contrast with the less than 8% for most SMA.[2]

Figure 5 presents the three-dimension (3D) diagram of the shape memory cycle of *c*PE for the first and eighth cycle and *c*PE/CB nanocomposites with v^{CB} of 5.0 and 20.0 vol % for the third cycle. Good reproducibility of SME can be seen for the *c*PE by comparing the first and eighth cycles. As also given in Table 1, high R_f (above 90% for v^{CB} below 10.0 vol %) and high R_r (above 99% for v^{CB} below 20.0 vol %) are achieved for all these three samples although R_f decreases slightly with increasing v^{CB}. As shown in Figure 5, it is very interesting to notice that, during the cooling in the second step, the ε still increases, which is a typical crystallization-induced elongation and has been used to obtain reversible SME.[20] The step corresponds to the crystallization of PE matrix duirng the cooling. During the heating in the fourth step, the ε decreases and the step corresponds to the melting of PE matrix. By comparing among these three samples, it can be seen that the ε change during the cooling and the subsequent heating becomes smaller with increasing v^{CB}. The reason is the decreased crysatllizability of PE matrix with increasing disturbance of CB nanoparticles.

Figure 6 presents the OM images showing the evolution of the scratch on the surface of *l*PE and *c*PE/CB nanocomposites with v^{CB} of 1.0 vol % during the heating process. As shown in Figure 6a,b, for the *l*PE, the width of the scratch only decreases slightly for the temperature up to 114.5 °C. However, for the *c*PE/CB nanocomposites with v^{CB} of 1.0 vol %, the width of the scratch has decreased significantly at 118.1 °C. These results indicate that the cross-linking of PE matrix favors the self-healing. Besides, the addition of CB nanoparticles also enhances this effect due to the increased E' as already shown in Figure 4. As shown in Figure 6c,d, for the nanocomposites with the scratch in the direction parallel to the previous stretching direction, there is still a noticeable scratch at 120.0 °C, while for the scratch in the direction perpendicular to the previous stretching direction, the scratch is almost gone at 120.2 °C. These results clearly indicate that the contraction of SMP materials during the heating in the direction perpendicular to

dx.doi.org/10.1021/jp3098796 | J. Phys. Chem. B 2013, 117, 1467−1474

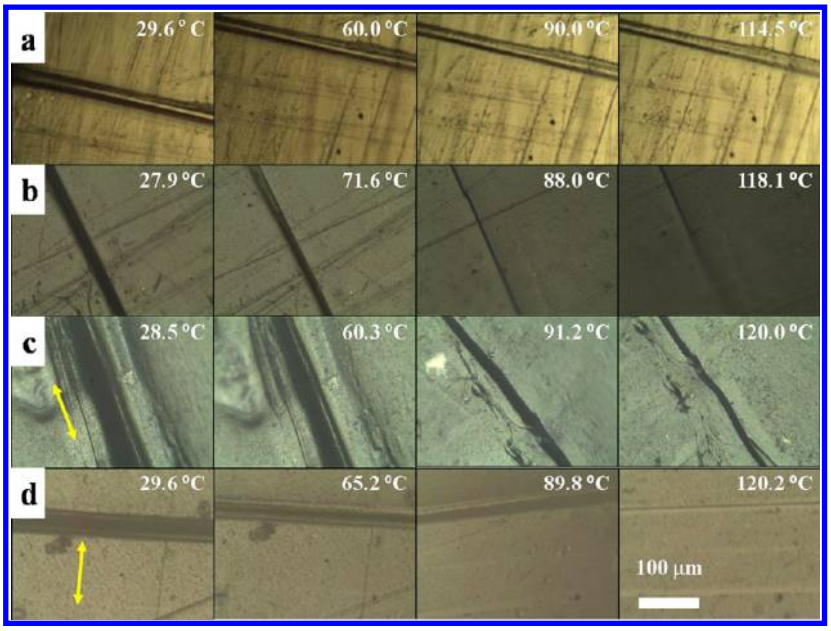

Figure 6. OM images showing the evolution of the scratch on the surface of *l*PE (a) and *c*PE/CB nanocomposites with ν^{CB} of 1.0 vol % (b–d) during the heating process at increasing temperatures as indicated. The samples in (a) and (b) are not stretched before the self-healing. The scratches in (c) and (d) are in the directions parallel and perpendicular to the previous stretching direction indicated as double-arrow lines, respectively.

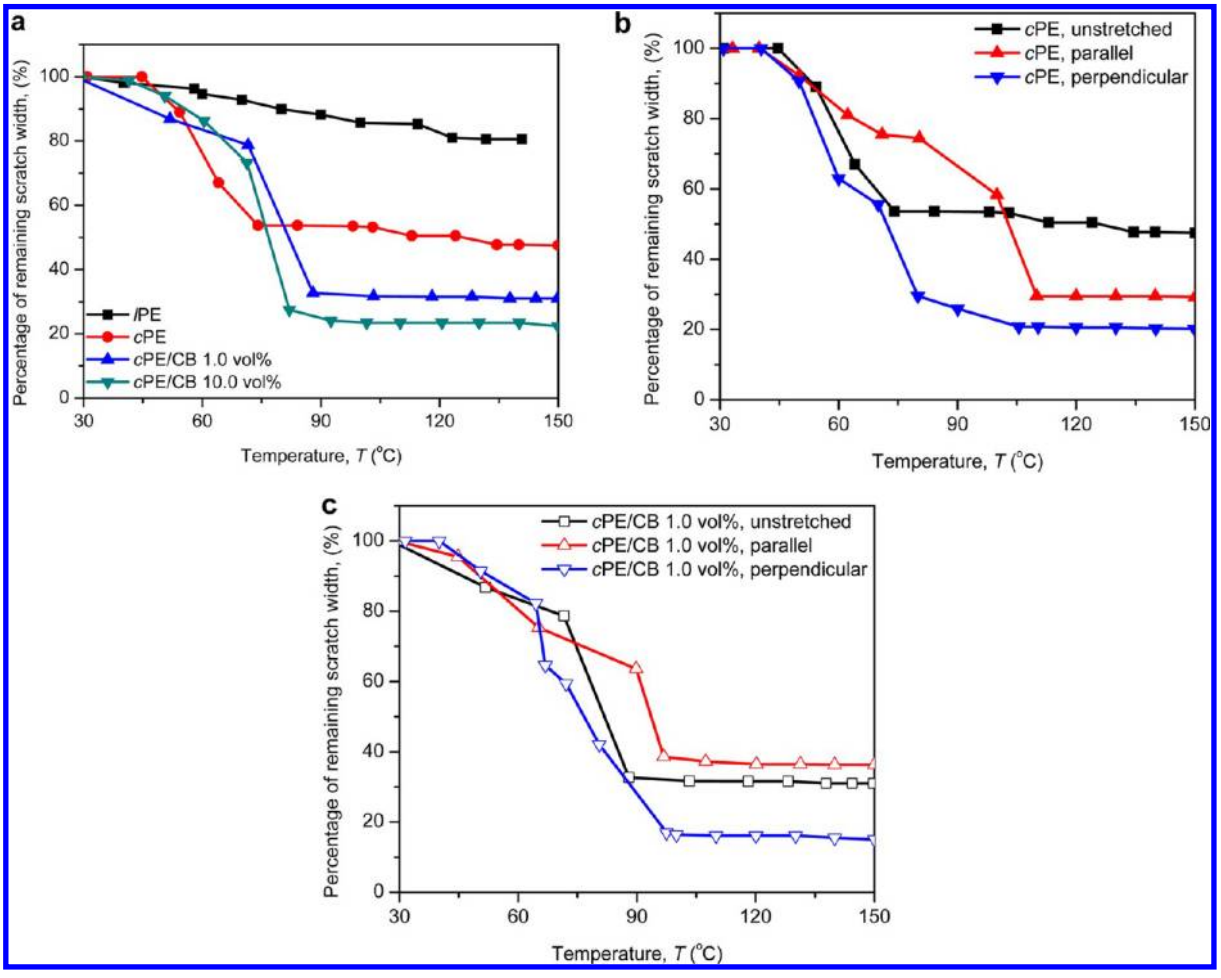

Figure 7. Temperature dependence of the percentage of remaining scratch width in *l*PE, *c*PE, and *c*PE/CB nanocomposites with various ν^{CB} (a), *c*PE (b), and *c*PE/CB nanocomposites with ν^{CB} of 1.0 vol % (c) with or without previous stretching. The solid lines in the figure are guides to the eyes.

dx.doi.org/10.1021/jp3098796 | J. Phys. Chem. B 2013, 117, 1467–1474

the scratch favors the closure of the scratch and the following self-healing by molecular interdiffusion. However, the contraction of SMP materials in the direction parallel to the scratch hinders the closure and the following self-healing.

Figure 7 presents the temperature dependence of the percentage of remaining scratch width in different samples with or without previous stretching. As shown in Figure 7a, for the samples without previous stretching, both the cross-linking of PE matrix and the addition of the CB nanoparticles favor the self-healing of PE matrix. As shown in Figure 7b, for the *c*PE samples, although the previous stretching in the direction both parallel and perpendicular to the scratch produces better closure of the scratch at upper limit temperature of 150.0 °C, the previous parallel stretching hinders the scratch closure at temperature up to temperature of ca. 100 °C. As shown in Figure 7c, for the *c*PE/CB nanocomposites with v^{CB} of 1.0 vol %, the previous stretching in the direction parallel to the scratch hinders the closure of the scratch, while the perpendicular stretching favors the scratch closure. Clearly, this SME-aided self-healing is dependent on the previous stretching with respect to the scratch direction.

CONCLUSIONS

The improved self-healing of *c*PE/CB nanocomposites by their SME has been achieved in this work. CB nanoparticles were found to be homogeneously dispersed in the PE matrix and significantly increase the strength of the materials. Compared with the breaking of *l*PE at the T_m, the *c*PE and *c*PE/CB nanocomposites still had high strength above T_m due to the formation of networks. The *c*PE and *c*PE/CB nanocomposites showed both high R_f and high R_r. Crystallization-induced elongation was observed for all the SMP materials and the effect became less remarkable with increasing v^{CB}. The scratch self-healing tests showed that the cross-linking of PE matrix, the addition of CB nanoparticles, and the previous stretching in the direction perpendicular to the scratch favored the closure of the scratch and its complete healing. This SME-aided self-healing could have potential applications in diverse fields such as coating and structure materials.

AUTHOR INFORMATION

Corresponding Author

*E-mail: junzhao@ustb.edu.cn. Tel.: +86 10 6233 4516. Fax: +86 10 6233 2599.

Notes

The authors declare no competing financial interest.

ACKNOWLEDGMENTS

This work was financially supported by Beijing Municipal Excellent Scholars (2011D009006000005), Open Topic Funding of Beijing National Laboratory for Molecular Sciences, NSF of China (Grant Nos. 50977001 and 51073015), The Ministry of Sciences and Technology of China through China-Europe International Incorporation Project (Grant No. 2010DFA51490), State Key Laboratory of Power System (SKLD11KZ04), and the Fundamental Research Funds for the Central Universities (Nos. 06103011 and 06103012).

REFERENCES

(1) Wu, D. Y.; Meure, S.; Solomon, D. Self-Healing Polymeric Materials: A Review of Recent Developments. *Prog. Polym. Sci.* **2008**, *33*, 479−522.

(2) Xie, T. Recent Advances in Polymer Shape Memory. *Polymer* **2011**, *52*, 4985−5000.

(3) Liu, C.; Qin, H.; Mather, P. T. Review of Progress in Shape-Memory Polymers. *J. Mater. Chem.* **2007**, *17*, 1543−1558.

(4) Zhang, H.; Wang, H.; Zhong, W.; Du, Q. A Novel Type of Shape Memory Polymer Blend and the Shape Memory Mechanism. *Polymer* **2009**, *50*, 1596−1601.

(5) Voit, W.; Ware, T.; Dasari, R. R.; Smith, P.; Danz, L.; Simon, D.; Barlow, S.; Marder, S. R.; Gall, K. High-Strain Shape-Memory Polymers. *Adv. Funct. Mater.* **2010**, *20*, 162−171.

(6) Lendlein, A. Progress in Actively Moving Polymers. *J. Mater. Chem.* **2010**, *20*, 3332−3334.

(7) Behl, M.; Razzaq, M. Y.; Lendlein, A. Multifunctional Shape-Memory Polymers. *Adv. Mater.* **2010**, *22*, 3388−3410.

(8) Meng, Q.; Hu, J. A Review of Shape Memory Polymer Composites and Blends. *Compos. Part A: Appl. Sci. Manuf.* **2009**, *40*, 1661−1672.

(9) Liu, Y.; Lv, H.; Lan, X.; Leng, J.; Du, S. Review of Electro-Active Shape-Memory Polymer Composite. *Compos. Sci. Technol.* **2009**, *69*, 2064−2068.

(10) Iijima, M.; Kobayakawa, M.; Yamazaki, M.; Ohta, Y.; Kamiya, H. Anionic Surfactant with Hydrophobic and Hydrophilic Chains for Nanoparticle Dispersion and Shape Memory Polymer Nanocomposites. *J. Am. Chem. Soc.* **2009**, *131*, 16342−16343.

(11) Xu, B.; Fu, Y. Q.; Ahmad, M.; Luo, J. K.; Huang, W. M.; Kraft, A.; Reuben, R.; Pei, Y. T.; Chen, Z. G.; De Hosson, J.; Th, M. Thermo-Mechanical Properties of Polystyrene-Based Shape Memory Nanocomposites. *J. Mater. Chem.* **2010**, *20*, 3442−3448.

(12) Xiao, X.; Xie, T.; Cheng, Y.-T. Self-Healable Graphene Polymer Composites. *J. Mater. Chem.* **2010**, *20*, 3508−3514.

(13) Golbang, A.; Kokabi, M. Temporary Shape Development in Shape Memory Nanocomposites Using Magnetic Force. *Eur. Polym. J.* **2011**, *47*, 1709−1719.

(14) Le, H. H.; Schoss, M.; Ilisch, S.; Gohs, U.; Heinrich, G.; Pham, T.; Radusch, H.-J. CB Filled EOC/EPDM Blends as a Shape-Memory Material: Manufacturing, Morphology and Properties. *Polymer* **2011**, *52*, 5858−5866.

(15) Bae, C. Y.; Park, J. H.; Kim, E. Y.; Kang, Y. S.; Kim, B. K. Organic-Inorganic Nanocomposite Bilayers with Triple Shape Memory Effect. *J. Mater. Chem.* **2011**, *21*, 11288−11295.

(16) Kumpfer, J. R.; Rowan, S. J. Thermo-, Photo-, and Chemo-Responsive Shape-Memory Properties from Photo-Cross-Linked Metallo-Supramolecular Polymers. *J. Am. Chem. Soc.* **2011**, *133*, 12866−12874.

(17) Zhang, S.; Feng, Y.; Zhang, L.; Sun, J.; Xu, X.; Xu, Y. Novel Interpenetrating Networks with Shape-Memory Properties. *J. Polym. Sci., Part A: Polym. Chem.* **2007**, *45*, 768−775.

(18) Neffe, A. T.; Hanh, B. D.; Steuer, S.; Lendlein, A. Polymer Networks Combining Controlled Drug Release, Biodegradation, and Shape Memory Capability. *Adv. Mater.* **2009**, *21*, 3394−3398.

(19) Serrano, M. C.; Carbajal, L.; Ameer, G. A. Novel Biodegradable Shape-Memory Elastomers with Drug-Releasing Capabilities. *Adv. Mater.* **2011**, *23*, 2211−2215.

(20) Chung, T.; Romo-Uribe, A.; Mather, P. T. Two-Way Reversible Shape Memory in a Semicrystalline Network. *Macromolecules* **2008**, *41*, 184−192.

(21) Bellin, I.; Kelch, S.; Lendlein, A. Dual-Shape Properties of Triple-Shape Polymer Networks with Crystallizable Network Segments and Grafted Side Chains. *J. Mater. Chem.* **2007**, *17*, 2885−2891.

(22) Kolesov, I. S.; Radusch, H.-J. Multiple Shape-Memory Behavior and Thermal-Mechanical Properties of Peroxide Cross-Linked Blends of Linear and Short-Chain Branched Polyethylenes. *Express Polym. Lett.* **2008**, *2*, 461−473.

(23) Xie, T. Tunable Polymer Multi-Shape Memory Effect. *Nature* **2010**, *464*, 267−270.

(24) Luo, X.; Mather, P. T. Triple-Shape Polymeric Composites (TSPCs). *Adv. Funct. Mater.* **2010**, *20*, 2649−2656.

(25) Ware, T.; Hearon, K.; Lonnecker, A.; Wooley, K. L.; Maitland, D. J.; Voit, W. Triple-Shape Memory Polymers Based on

Self-Complementary Hydrogen Bonding. *Macromolecules* **2012**, *45*, 1062−1069.
(26) White, S. R.; Sottos, N. R.; Geubelle, P. H.; Moore, J. S.; Kessler, M. R.; Sriram, S. R.; Brown, E. N.; Viswanathan, S. Autonomic Healing of Polymer Composites. *Nature* **2001**, *409*, 794−797.
(27) Keller, M. W.; White, S. R.; Sottos, N. R. Torsion Fatigue Response of Self-Healing Poly(dimethylsiloxane) Elastomers. *Polymer* **2008**, *49*, 3136−3145.
(28) Toohey, K. S.; Sottos, N. R.; Lewis, J. A.; Moore, J. S.; White, S. R. Self-Healing Materials with Microvascular Networks. *Nat. Mater.* **2007**, *6*, 581−585.
(29) Hayes, S. A.; Jones, F. R.; Marshiya, K.; Zhang, W. A Self-Healing Thermosetting Composite Material. *Compos. Part A: Appl. Sci. Manuf.* **2007**, *38*, 1116−1120.
(30) McGarel, O. J.; Wool, R. P. Craze Growth and Healing in Polystyrene. *J. Polym. Sci., Part B: Polym. Phys.* **1987**, *25*, 2541−2560.
(31) Chen, X.; Dam, M. A.; Ono, K.; Mal, A.; Shen, H.; Nutt, S. R.; Sheran, K.; Wudl, F. A Thermally Re-mendable Cross-Linked Polymeric Material. *Science* **2002**, *295*, 1698−1702.
(32) Cordier, P.; Tournilhac, F.; Soulie-Ziakovic, C.; Leibler, L. Self-Healing and Thermoreversible Rubber from Supramolecular Assembly. *Nature* **2008**, *451*, 977−980.
(33) Varley, R. J.; van der Zwaag, S. Towards an Understanding of Thermally Activated Self-Healing of an Ionomer System during Ballistic Penetration. *Acta Mater.* **2008**, *56*, 5737−5750.
(34) Montarnal, D.; Tournilhac, F.; Hidalgo, M.; Couturier, J.-L.; Leibler, L. Versatile One-Pot Synthesis of Supramolecular Plastics and Self-Healing Rubbers. *J. Am. Chem. Soc.* **2009**, *131*, 7966−7967.
(35) Zheng, P.; McCarthy, T. J. A Surprise from 1954: Siloxane Equilibration Is a Simple, Robust, and Obvious Polymer Self-Healing Mechanism. *J. Am. Chem. Soc.* **2012**, *134*, 2024−2027.
(36) Li, G.; Nettles, D. Thermomechanical Characterization of a Shape Memory Polymer Based Self-Repairing Syntactic Foam. *Polymer* **2010**, *51*, 755−762.
(37) Nji, J.; Li, G. A Biomimic Shape Memory Polymer Based Self-Healing Particulate Composite. *Polymer* **2010**, *51*, 6021−6029.
(38) Rodriguez, E. D.; Luo, X.; Mather, P. T. Linear/Network Poly(ε-caprolactone) Blends Exhibiting Shape Memory Assisted Self-Healing (SMASH). *ACS Appl. Mater. Inter.* **2011**, *3*, 152−161.
(39) Kolesov, I. S.; Kratz, K.; Lendlein, A.; Radusch, H.-J. Kinetics and Dynamics of Thermally-Induced Shape-Memory Behavior of Crosslinked Short-Chain Branched Polyethylenes. *Polymer* **2009**, *50*, 5490−5498.
(40) Kaushik, A. K.; Podsiadlo, P.; Qin, M.; Shaw, C. M.; Waas, A. M.; Kotov, N. A.; Arruda, E. M. The Role of Nanoparticle Layer Separation in the Finite Deformation Response of Layered Polyurethane-Clay Nanocomposites. *Macromolecules* **2009**, *42*, 6588−6595.